

Article

Start-Up of a Solid Oxide Fuel Cell System with a View to Materials Science-Related Aspects, Control and Thermo-Mechanical Stresses

Konrad W. Eichhorn Colombo * and Vladislav V. Kharton

Institute of Solid State Physics Russian Academy of Sciences, Chernogolovka, 142432 Moscow, Russian; kharton@issp.ac.ru

* Correspondence: konrad.eichhorn@issp.ac.ru

Abstract: The start-up of a solid oxide fuel cell (SOFC) is investigated by means of numerical simulation with a view to material and operational constraints on a component and system level, as well as thermo-mechanical stresses. The applied multi-physics modeling approach couples thermal-, electrochemical, chemical-, and thermo-mechanical phenomena. In addition to constraints, emphasis is given to degrees of freedom with respect to manipulated and controlled variables of the system. Proper ramping during the start-up procedure keeps critical parameter values within a safe regime. Of particular interest are gradient in terms of temperature and chemical concentrations. Nevertheless, simulations show that thermo-mechanical stresses are relatively high during the initial start-up phase, the system is, thus, more susceptible to failure. The combination of multi-physics modeling in conjunction with practical control aspects for start-up of an SOFC, which is presented in this paper, is important for applications.

Keywords: solid oxide fuel cell system; start-up; multi-physics; mathematical modeling; constraints; process control



Citation: Eichhorn Colombo, K.W.; Kharton, V.V. Start-Up of a Solid Oxide Fuel Cell System with a View to Materials Science-Related Aspects, Control and Thermo-Mechanical Stresses. *Crystals* **2021**, *11*, 732. <https://doi.org/10.3390/cryst11070732>

Academic Editors: Shujun Zhang, Helmut Cölfen, Abel Moreno, Charles Rosenblatt and Sławomir Grabowski

Received: 5 May 2021
Accepted: 11 June 2021
Published: 24 June 2021

Publisher's Note: MDPI stays neutral with regard to jurisdictional claims in published maps and institutional affiliations.



Copyright: © 2021 by the authors. Licensee MDPI, Basel, Switzerland. This article is an open access article distributed under the terms and conditions of the Creative Commons Attribution (CC BY) license (<https://creativecommons.org/licenses/by/4.0/>).

1. Introduction

Fuel cells (FC) are an important part of the sustainable power generation mix [1], also as elements of larger system networks [2], and for vehicles [3]. Various FC technologies have been developed [4], where solid oxide fuel cells (SOFC) have certain advantages in comparison to other FC types, for example the potential use of non-precious metals [5], which have therefore been intensively investigated [6–8]. Nevertheless, issues remain to obtain sufficient lifetime for a wide application, including irreversible degradation of electrodes, electrolyte, and sealing materials linked to the fuel contaminants (further discussed below) [9–14].

Mathematical modeling is indispensable to gain insights about performance for realistic and critical scenarios of complex systems due to mutual interaction of time-dependent physical phenomena as well as strong dependence on operation conditions. In addition to an electro-chemical perspective to assess thermodynamic performance, a systems perspective should also take into account thermo-mechanical aspects [15–17] to analyze overall metrics that specify the system lifetime.

Benign operation conditions in terms of transient gradients already lead to complex control strategies due to the number of physical variables that need to be controlled as well as material and operational constraints. For safe and economically feasible system start-up, further aspects need to be addressed [18,19], for example due to the need for safety gas [20] to maintain proper conditions with respect to chemical potential in the material to avoid excessive stresses during rapid transients. However, compared to studies that are concerned with design point performance and off-design (including part-load operation), relatively few publications exist dealing with detailed transient behavior on a system level.

Even fewer studies directly investigate the start-up behavior with all the aforementioned physical phenomena (see References [21,22], and in particular those conducted by the Jülich team [23–25]), despite the critical importance of these aspects. Of special interest are gradients in temperature, as well as chemical compositions.

The multi-physics approach with time-dependent partial differential algebraic integral equations (PDAIE) is a core element of a more general model-based systems engineering (SE) framework (See also Reference [26] for a recent review comparing characteristic specifications of electro-chemical energy systems). Systems control is another branch within this model-based SE framework, where simplified models in the frequency- or time domain are commonly used to develop control strategies and to tune controllers, e.g. based on (nonlinear) model predictive control [27]. To obtain information about a system's transient behavior subject to disturbances, (open-loop) step responses are imposed. The underlying models are however in many cases linear, or more general, reduced order representations, of a high-fidelity or simplified physics-based model. Besides, control objectives may be in mutual conflict. In summary, the model-based SE framework used in this work balances the physics- and control perspective to arrive at a more realistic understanding of failure-induced risks for the SOFC during start-up, compared to a purely thermodynamic (equilibrium) performance approach. With a broader and more detailed perspective, better conclusions and actions can be formulated for practical operating systems, their control and economics.

To the best of our knowledge, the present study is one of few which investigates SOFC behavior on a component and system level during start-up by means of a thermo-mechanical model in conjunction with physics-based control constraints.

A separate note on system shutdown is necessary. For a normal shutdown, i.e., no emergency shutdown, the inverse of the start-up procedure is assumed to be applicable, possibly with some adjustments in terms of duration for the individual operation phases. In the following, only start-up is considered where normal shutdown proceeds in the same (or similar) fashion.

2. System Description

2.1. Solid Oxide Fuel Cell

In this work, one of the most basic SOFC-based system designs is assumed, shown in the process flow diagram in Figure 1. Hydrogen and air are fed to the SOFC where it is converted to electrical DC power. Any remaining hydrogen is burned in the combustor afterwards, which provides further heat to the process system. This heat is utilized to pre-heat the gas streams which consist of oxygen-depleted air and steam. The electrical DC power is converted to AC power by means of a converter. Hydrogen is assumed as feedstock because it is perhaps the most benign fuel for SOFC and also other fuel cell types. More complex feedstocks would require further auxiliary equipment and also add more constraints. Probably some more fundamental and pressing issues need to be resolved first for such basic system designs which will also be present in more complex designs, such as level of heat integration and operational requirements including the choice of fuel. The general auxiliary system equipment which is required for start-up is also indicated (in blue in Figure 1), further piping and instrumentation may also be needed.

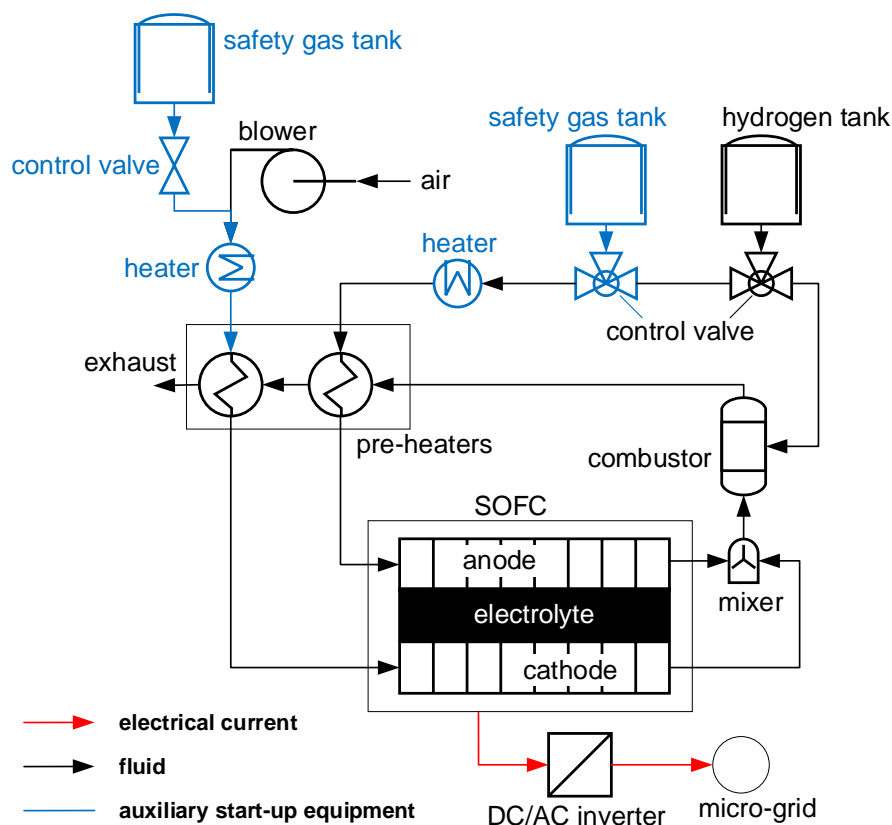


Figure 1. Basic SOFC system design with auxiliary equipment for start-up and shutdown (in blue).

2.2. Principal System Operation and Design

The principal mechanism in an individual SOFC is shown in Figure 2 with the gas channels and composite layers as its main parts. In addition to that, metallic current collectors (interconnects) and sealants are required (not shown in the figure). The gas channels on the cathode side provide the fluid for reduction and those on the anode side for oxidation, respectively. An oxygen-ion conducting solid electrolyte separates the cathode and anode. The outer electrical circuit provides charge neutrality and movement of electrons.

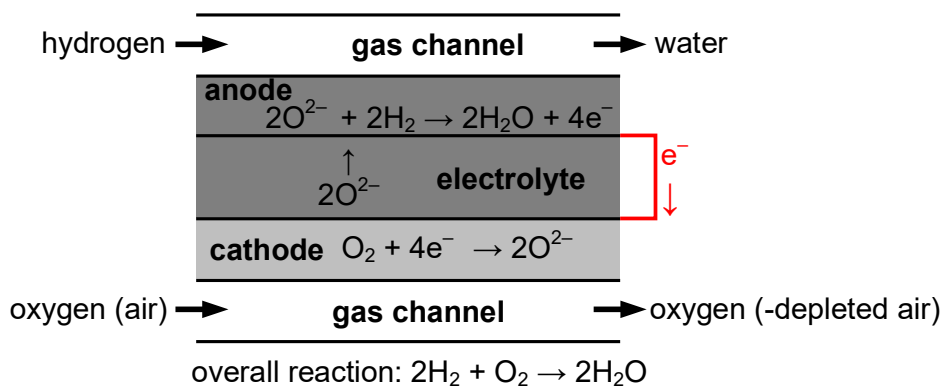
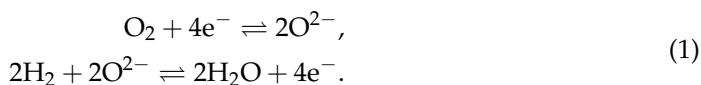


Figure 2. Principle of a solid oxide fuel cell.

Oxygen ions move from the cathode across the electrolyte membrane to the anode with the half-cell reactions on the cathode (oxygen reduction) and anode (fuel oxidation) [4]



The SOFC is assumed to be of tubular-type, as shown in Figure 3 [28–30], with a total number of 1.200 equally behaving cells. Note that other geometries are also possible, such as planar designs, which have specific advantages and drawbacks compared to the tubular design [31,32]. Furthermore, designs may also differ with respect to cell-support. Here, a design with supporting cathodes was considered, but there are also designs with anode- and electrolyte-supported cells. Cathode-supported cells were reported to have advantages in terms of low carbon deposition [33] and, thus, fuel flexibility. Another advantage is the potentially lower risk of Ni-oxidation which leads to better mechanical integrity [34]. The cathode-supported SOFC may be regarded as optimal choice in terms of support thickness and operating parameters [35,36]. A drawback, compared to electrolyte- and anode-supported configurations, is a high polarization resistance [33]. Reference [37] provides further information about the present design.

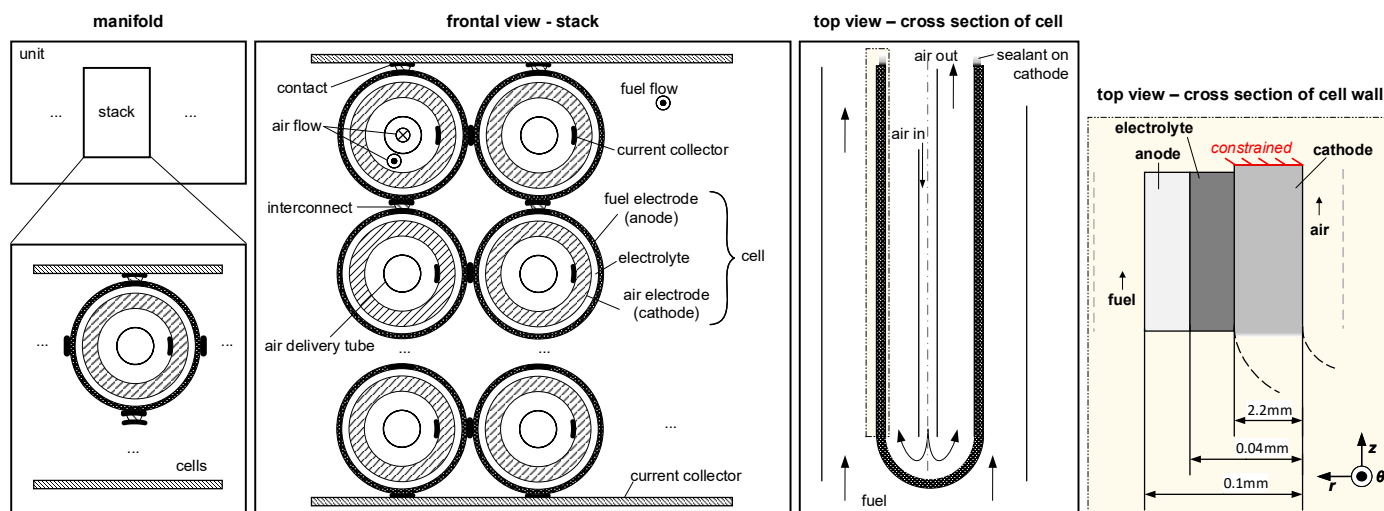


Figure 3. SOFC design.

2.3. Design and Operation System Constraints

Table 1 summarizes critical design and operation constraints of the SOFC-based system that determine the overall operation envelope for the SOFC. Of particular relevance are constraints related to temperature gradients which determine thermo-mechanical stresses. Note that constraints for the balance-of-plant system components are also shown for completeness. Some of those may be disregarded during start-up because of the use of auxiliary equipment. For example, the combustor is an active component which provides heat to the system. During start-up of the system, however, it may be necessary to use a secondary heat source in conjunction with auxiliary heaters to avoid potential fluctuations and rapid changes due to its relatively small thermal inertia [38]. In this work, setpoints of all manipulated variables are achieved without deviation and any constraints due to balance-of-plant system components are disregarded. Any preparation task for physical system start-up is assumed to be completed, including purging of gas channels. Furthermore, heat losses are likely to be of less concern during the relatively short start-up time compared to target operation times. Even though constraints may be soft with the principle possibility to exceed those, substantial performance loss, aggregation of irreversibilities, or both, may occur.

Table 1. Design and operation constraints.

Unit	Constraint	Potential Effect	Limit
system	heat loss	performance loss	per design
SOFC	power density	increasing currents lead to higher concentration polarization and faster cell degradation	80–90% [39–41]
SOFC	max. leakage rate (interconnects)	performance loss, failure due to leakage	0.1% [39–41]
SOFC	min. temperature	performance loss, and failure due to thermo-mechanical stresses	900 K [39–42]
SOFC	max. temperature	performance loss and failure due to thermo-mechanical stresses and chemical interaction	1300 K [39–41]
SOFC	max. difference in thermal expansion coefficients	performance loss and failure due to thermo-mechanical stresses	10–17% [39–41]
SOFC	transient temperature gradients	thermo-mechanical stresses	20 K/cm [43,44]
SOFC	steady state temperature differences in axial direction of SOFC	thermo-mechanical stresses	150 K [39–41]
SOFC	min. FU	thermo-mechanical stresses	40% [39–41]
SOFC	max. FU	fuel starvation, efficiency loss	90% [39–41]
SOFC	max. total pressure difference between fluid streams	mechanical stress	3 bar [39–41]
combustor	air excess ratio	performance loss, emissions, flame instability	6–12 [45]
combustor	residence time	flame instability, blowout [46–50]	
combustor	max. temperature	mechanical stress	1400 K [42,46,51]
pre-heater	max. temperature	loss of strength	1300 K [52]
blower	max. volume flow, pressure, rotational speed [53,54]	stress, flow instability, performance loss	defined by design
tank	max. pressure, discharge rate [55]	mechanical stress	
valve	speed, max. volume flow [56]		defined by design
controller, actuator	speed, accuracy [57]	delay times, setpoint shift	
sensor	uncertainty, accuracy	delay times, setpoint shift	

2.4. Degrees of Freedom

The controlled (CV) and manipulated variables (MV) for the SOFC system are listed in Table 2, also shown are the values for those related to the SOFC after more than 2 h from completion of the start-up procedure, i.e., when (semi-)steady state conditions can be assumed (further discussed below). The difference between the number of CV and MV represents the degrees of freedom (DOF) available in the system [58] but other options may also be possible for some of the variables. The selection of variables and their pairing need to take into account the general measurability of a quantity and its response time. For example, electrical properties, such as electrical current, usually respond faster than those related to heat. In the presence of electrochemically reactive species in the reaction zone (triple-phase-boundaries (TPB)) the SOFC can respond to load variations within the time scale of electrochemistry [38].

A physics-based system modeling approach requires to establish a well-posed formulation of the mathematical problem, which can be utilized to identify the correct set of CV and MV, both from a physical as well as technological perspective. The emerging required

input parameters, therefore, represent exactly the DOF. For example, values of spatially distributed system state variables are usually not (easily) accessible through direct measurement, nevertheless, overall system state variables can be defined. A case in point is the mean solid temperature of the SOFC (defined below) which is a quantity obtained through numerical integration. Such metrics that are based on detailed models provide a better description of system constraints and operation compared to lumped-per-default quantities.

Well-posedness of the mathematical problem for numerical solution is preserved, independently whether MV or CV are specified as input parameters. In this respect, specifying the CV corresponds to the case of perfect control without deviations in measurements of MV, controller actions for CV, or other stochastic effects.

Table 2. Set of CV and MV.

Controlled Variable	Value	Manipulated Variable	Value
electrical system power	86.73 kW	electrical current	131.1 A
mean solid temperature of SOFC	1261 K	molar flow of air (blower capacity)	18 mol s ⁻¹
FU of SOFC	71.5%	molar flow of fuel to SOFC (fuel valve opening)	1.15 mol s ⁻¹
pressure gradient across solid of SOFC	<0.1 bar	use of throttles (not shown in Figure 1)	-
combustion outlet temperature	-	fuel mass flow to combustor (fuel valve opening)	-
air temperature to SOFC	-	bypass ratio of air (not used here)	-
driving force for chemical kinetics in SOFC	-	fuel composition (not used here)	-

3. Mathematical Model

In this section, the mathematical model of the SOFC is briefly presented. The connection between the thermo-electrochemical-chemical performance and thermo-mechanical stress sub-models is shown in Figure 4, where the temperature field of the solid is calculated in the performance model and simultaneously used as input for the stress model. In the latter, the tensor stress field is determined. References [59,60] provide further details. And a complete description of the thermo-mechanical steady state model (including boundary conditions) is given in references [61,62].

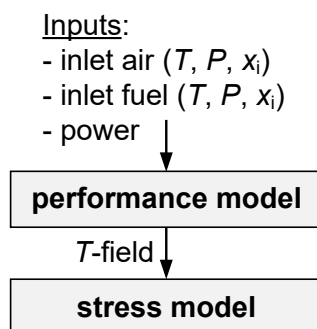


Figure 4. Link between the thermo-electrochemical-chemical performance model and thermo-mechanical stress model.

3.1. Energy and Mass Conservation

Heat transfer for gas and solid, respectively, are described by [59,60,63]

$$\frac{\partial T_g c_{p,g} \rho_g}{\partial t} + v_g \frac{\partial T_g c_{p,g} \rho_g}{\partial z} = \frac{2h_c}{r} (T_s - T_g), \quad (2)$$

$$\rho_s c_{p,s} \frac{\partial T_s}{\partial t} = \lambda_s \nabla^2 T_s. \quad (3)$$

with the boundary condition [59,60]

$$\lambda_s \frac{\partial T_s}{\partial r} = h_c (T_s - T_g) + \frac{\dot{r} \Delta h}{2\pi r L}, \quad (4)$$

where the reaction rate is given by [4]

$$\dot{r} = \frac{iA}{2F}. \quad (5)$$

For the gas phases, mass conservation reads [59,60,63]

$$\frac{\partial C_i}{\partial t} + v_g \frac{\partial C_i}{\partial z} = \dot{r}_i, \quad (6)$$

The model includes pressure drops for the gas streams.

3.2. Electrochemistry

The cell voltage is [4,29]

$$V_{\text{cell}} = V_{\text{OC}} - \eta_{\text{act}}^{\text{an}} - \eta_{\text{act}}^{\text{ca}} - \eta_{\text{con}}^{\text{an}} - \eta_{\text{con}}^{\text{ca}} - \eta_{\text{ohm}} \quad (7)$$

The Nernst equation gives the open circuit voltage (OCV) [4,29]

$$V_{\text{OC}} = E^\circ + \frac{RT}{zF} \ln \frac{a_{\text{oxi}}}{a_{\text{red}}}. \quad (8)$$

And with the Butler-Volmer equation the activation polarization losses are implicitly determined [4,29]

$$i_i = i_i^\circ \left[\exp\left(\frac{n_i \beta_{\text{fi}} F \eta_{\text{act},i}}{RT}\right) - \exp\left(-\frac{n_i \beta_{\text{ri}} F \eta_{\text{act},i}}{RT}\right) \right] \quad (9)$$

The concentration polarization losses are described as follows [4,29]

$$\eta_{\text{con},i} = \frac{RT}{n_i F} \ln(p_{i,g}, p_{i,\text{TPB}}). \quad (10)$$

The ohmic loss is [4,29]

$$\eta_{\text{ohm}} = iAR, \quad (11)$$

with an ohmic resistance comprising temperature-dependent layer resistivity of electrodes and electrolyte and a constant resistivity for the interconnects [59,60].

3.3. Thermo-Mechanics of Solid Components

The deformations and displacements of the solid material are determined by means of the Navier equations in cylindrical coordinates [64,65]

$$\begin{aligned} \mu \left(\nabla^2 u_r - \frac{u_r}{r^2} \right) + (\lambda + \mu) \frac{\partial}{\partial r} \left(\frac{1}{r} \frac{\partial}{\partial r} (r u_r) + \frac{\partial u_z}{\partial z} \right) &= \beta \frac{\partial \tilde{T}}{\partial r}, \\ \mu \nabla^2 u_z + (\lambda + \mu) \frac{\partial}{\partial z} \left(\frac{1}{r} \frac{\partial}{\partial r} (r u_r) + \frac{\partial u_z}{\partial z} \right) &= \beta \frac{\partial \tilde{T}}{\partial z}. \end{aligned} \quad (12)$$

The relations between displacement and strain are [65]

$$\begin{aligned}\varepsilon_r &= \frac{\partial u_r}{\partial r}, \\ \varepsilon_\theta &= \frac{u_r}{r}, \\ \varepsilon_z &= \frac{\partial u_z}{\partial z}, \\ \varepsilon_{zr} = \varepsilon_{rz} &= \frac{1}{2} \left(\frac{\partial u_r}{\partial z} + \frac{\partial u_z}{\partial r} \right).\end{aligned}\quad (13)$$

Stress and strain are related through Hooke's law [65]

$$\begin{aligned}\sigma_i &= \lambda(\varepsilon_r + \varepsilon_\theta + \varepsilon_z) + 2\mu\varepsilon_i - \beta\tilde{T}, \text{ with } i = r, \theta, z, \\ \tau_{zr} &= \tau_{rz} = 2\mu\varepsilon_{zr}.\end{aligned}\quad (14)$$

Boundary conditions are defined at gas–solid and solid–solid interfaces. One end is assumed to be fixed on the cathode and the other end is free [59,60], as shown in Figure 3. The crooks (indicated by dotted lines in the top view of Figure 3) for individual cells are not included in the present analysis because these are assumed to be less susceptible to failure compared to the electro-chemically active materials of the electrodes and electrolyte. Furthermore, the use of current collectors as indicated in Figure 3, represent a discontinuity of the tubes, their effects are also disregarded here. Note that a variety of materials have been developed for the individual parts of the SOFC, see for examples references [66,67] for individual advantages and drawbacks, also including the materials assumed in this work.

Thermo-mechanical parameters are [64,65]

$$\begin{aligned}\lambda(z) &= \frac{E(z)\nu}{(1+\nu)(1-2\nu)}, \\ \mu(z) &= \frac{E(z)}{2(1+\nu)}, \\ \beta(z) &= \frac{\alpha E(z)}{1-2\nu}.\end{aligned}\quad (15)$$

The initial stress distribution during the sintering process, with a reference temperature of 1473 K [68], is assumed to be homogeneously distributed in the material. See Table 3 for additional input parameters.

Table 3. Thermo-elastic input parameters.

Component	Material	E [GPa]	ν [-]	α [$10^{-6} \cdot \text{K}^{-1}$]
anode (reduced)	Ni-3YSZ	$f_2(T)$ [69]	0.387 [69]	12.6
electrolyte	8YSZ	$f_3(T)$ [69]	0.31 [69]	10.9 [69]
cathode	LSM	41 [70]	0.28 [70]	12 [71]

3.4. System Variables

The total current from the SOFC is

$$I = \frac{A}{L} \int_0^L i(z) dz, \quad (16)$$

with the DC power

$$P = VI. \quad (17)$$

Fuel utilization (FU) is calculated according to [4]

$$FU = \frac{I}{2F\dot{n}_{\text{fuel}}}. \quad (18)$$

The overall electrical system efficiency is

$$\eta_{\text{el}} = \frac{P}{\dot{n}_{\text{fuel}}LHV_{\text{fuel}}}. \quad (19)$$

And the mean solid temperature is determined by

$$\bar{T}_s = \frac{1}{L} \int_0^L T_s(z) dz. \quad (20)$$

3.5. Degradation and Failure Mechanisms

Potential degradation mechanisms for SOFC are numerous, complex, and often mutually dependent. For example, the system design determines to some extent which mechanisms will be dominant [72], also the actual dimensions of parts [73]. Materials the process components and parts are made of are other design criteria with a strong effect on performance and durability [41]. The feed-gases, in particular the fuel and its purity, are further criteria (see also references in the introduction). For example, carbon-containing fuels, such as natural gas or synthetic gas (produced from biomass or coal gasification), can lead to coke formation [74]. Sulfur, even in relatively small amounts, can promote poisoning [75]. Moreover, evaporation of materials from balance-of-plant system components may also cause contamination. The complex kinetics are temperature-dependent (among others), operation conditions therefore also strongly affect degradation mechanisms, for example in terms of voltage, current density and FU [76]. Yet another criterion with an effect on materials durability is the number of cycles the system undergoes as well as their characteristics in terms of loads and dynamics [77].

In this work, the gas supplied to the SOFC is assumed to be free of any potential contaminants. Safety gas is used for the simulation to control the electrochemical reactions and chemical potential, respectively. In addition, uncertainties would be introduced, since in many cases data are not available for the entire range of interest for start-up analysis, which must cover a temperature range from ambient temperature to the temperature ranges required for operation.

Failures can occur as a result of thermo-mechanical stresses, with a force-term comprising temperature gradients and differences between the materials with respect to physical properties, such as thermal expansion coefficients (see Table 3). It is emphasized that degradation mechanisms can also promote or trigger failures, for example due to material defects that are introduced during manufacture or system assembly. However, these effects are characterized by high stochastics and can hardly be captured with first principles modeling.

3.6. Model Implementation and Numerical Solution Methods

The model was implemented and numerically solved in gPROMS [78]. Besides well-posedness, the solution requires a problem formulation of index one (The index determines the smallest number of times the PDAIE must be differentiated to determine continuous functions of the state variables and certain space derivatives of their components. The higher the index, the more difficult it is to solve the equation system. Individual equations may be reformulated if models have an index higher than one for the numerical solvers to handle.).

Finite difference (FD) schemes are used for the discretization of the PDE. For the SOFC 40 discretization elements in axial direction and 10 in radial direction for the cathode, and 5 for the anode and electrolyte are used (cathode is the thickest part of the assembly). The total number of equations for the complete system is 14.5 k (13 k algebraic and 1.5 k differential equations). The thermodynamic model was tested with a finer discretization, which led to

a higher number of equations and therefore computation time but little difference in the results. Backward, forward and central FD methods were used for discretization. Air in the air delivery tube used backward FD, whilst for the air and fuel forward FD was used as they have the same flow direction. Central FD was used for the solid membrane layer. All simulations start with steady state as initial condition. As the numerical solution of strongly coupled time-dependent PDAIE systems are demanding for the solvers, in particular in the presence of (imposed) discontinuities and a wide parameter value range for state variables, various techniques were used for numerical stability, including non-dimensionalizations and adjustments of solver settings.

The physical property package Multiflash [78], is used for thermodynamic properties, while thermo-mechanical properties were taken from literature (e.g., Table 3). Empirical functions were implemented for continuous parameter-dependency using the software DataFit [79].

4. Results and Discussion

4.1. Model Verification and Thermodynamic Steady State Performance

The overall deviation of energy and mass conservation due to the numerical solution between the inlets and outlets on a component- and system level

$$\Delta\zeta = 1 - \frac{\sum_k \zeta_{in,k}}{\sum_k \zeta_{out,k}}, \quad \zeta = \dot{E}, \dot{m}, \quad (21)$$

to verify the model for all steady state simulation. For the energy balance check of the SOFC the supplied heat through the feed gas, as well as electrochemical reactions need to be taken into account. The deviation with respect to energy is about 0.1% and for mass about 0.001%, which is considered as sufficiently small.

The original thermodynamic model is based on References [59,60], which was validated against results from cited references. For the thermo-mechanical part, a direct validation of simulation results presented in this work was not possible, neither a comparison with other works using the same assumptions, such as geometry, reference temperature, and operating conditions. However, results for stresses and displacement presented below are comparable with those reported in other studies, see Table 4.

Table 4. Comparison of simulation results for electrolyte against literature data.

Parameter	This Study	Ref. [80,81]
approximate max. abs. displacement (z) [mm]	1.3	1.34
approximate max. abs. displacement (r) [mm]	0.04	0.5
approximate max. abs. axial stress [MPa]	330	265–583

Figure 5 shows results for current density and solid temperature from the thermodynamic performance model under normal operation conditions, with a voltage of 0.55 V, after more than 15 h from initiating start-up (see Figures 6 and 7), the mean solid temperature is 1261 K (Table 2). As shown in Figure 3, air is preheated in the air delivery tubes. Heat transfer between the preheated air and fuel, which flow in the same direction, is determined by convection in addition to heat generation through electrochemical reactions (Figure 2). Due to this heat source, the solid temperature (electrodes and electrolyte) is close or even higher (but still <1 K) than that of the fuel temperature, rather than between the gases (temperature profiles are not shown). Hydrogen and steam in the fuel, and oxygen in the depleted air, participate in the electrochemical reactions. The current density is calculated through the reaction rate (not shown), which is a function of the solid temperature and the driving force caused by the electrochemically reacting species. It ranges from 0.402 to 0.498 Acm⁻², i.e., current density is relatively homogeneously distributed over the axial direction. The resulting total electrical current for the system is 131.1 A (Table 2). The drop

in current density after passing the mid section (from right to left) is dominated by the decreasing driving force in axial direction in spite of higher solid temperatures.

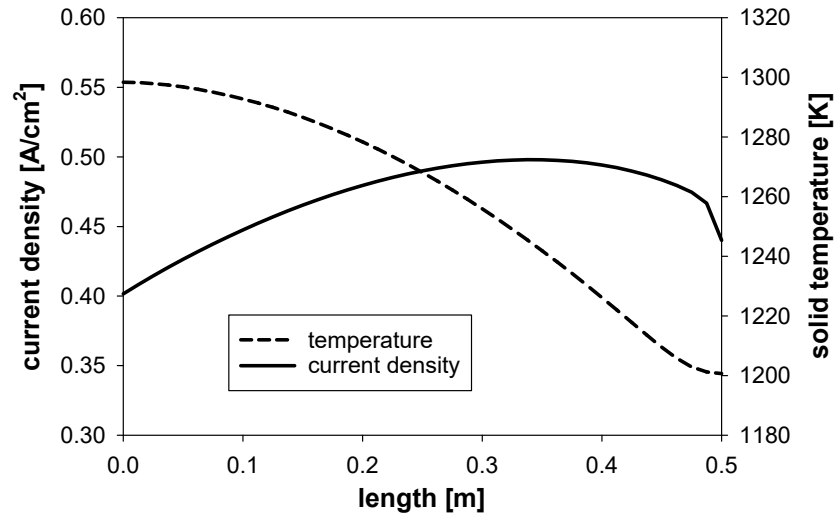


Figure 5. Current density and solid temperature under normal operation conditions.

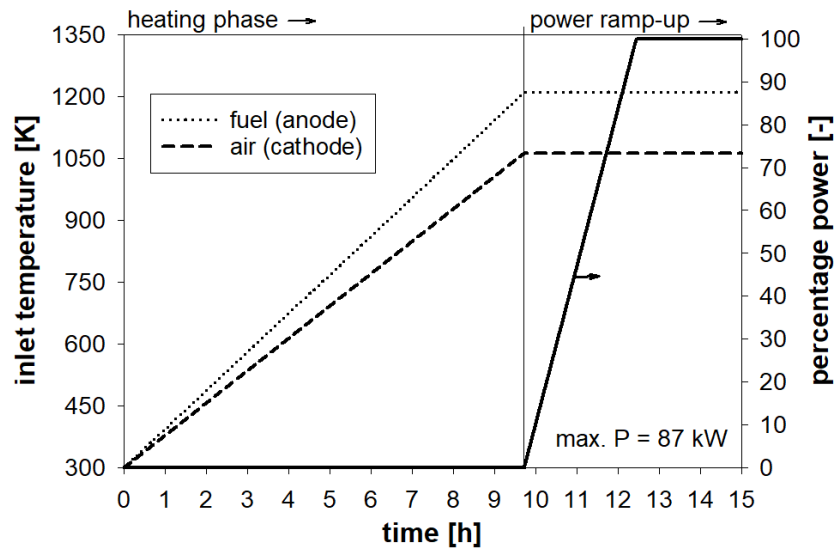


Figure 6. Ramping of fluid temperatures and power.

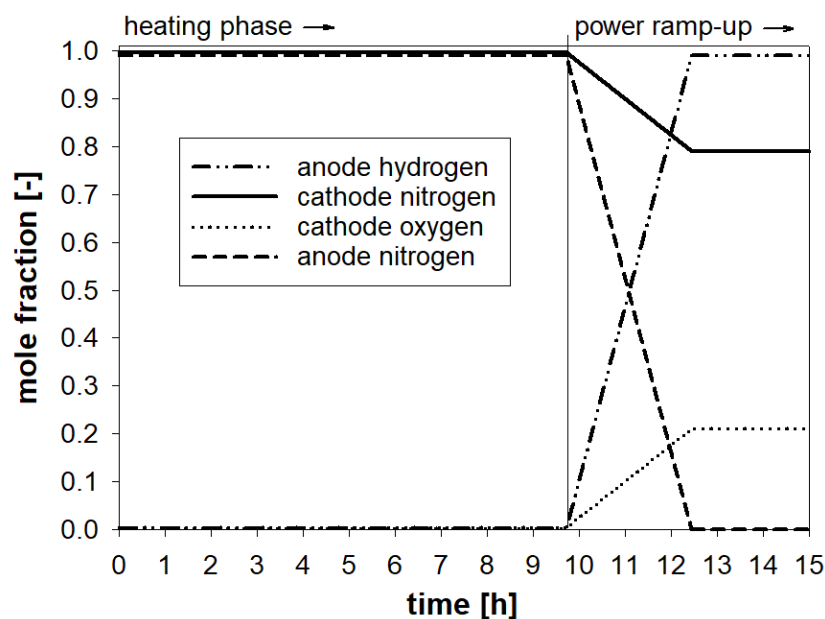


Figure 7. Ramping of fluid compositions.

4.2. Start-Up Procedure

The start-up procedure consists of two phases, namely heating and power-ramping. In the heating phase the system's temperature is increased by auxiliary heaters; the resulting temperature profiles are shown in Figure 6 (see also the system block diagram in Figure 1). During this phase no electrical power is extracted from the system. Heat transfer through anode and cathode gas is used to increase the temperature in the SOFC at a rate of 1.308 Kmin^{-1} for air and 1.56 Kmin^{-1} for fuel, respectively. A higher rate, and, thus, final maximum temperature, was chosen for the fuel gas based on the target design point [82], but other temperatures and combinations with respect to temperature differences between the feed gas streams are in principle also possible. The start-up procedure is initiated under non-reactive conditions at ambient temperature and ends when target operation conditions are reached with respect to the controlled variables (see Table 2). In the second phase, the chemical compositions of the two feed gas streams are changed, as shown in Figure 7 (anode hydrogen up and nitrogen down, cathode oxygen up and nitrogen down), along with power ramp-up (531 Wmin^{-1}) (Figure 6) until the target design point has been reached. This safety gas is used for the anode, as well as cathode to control the hydrogen and oxygen partial pressures, respectively. The mass flows are kept constant for simplicity but they are additional DOF, which are important from an economic point of view. Various scenarios were simulated for the ramping of gas compositions and electrical power. In this work, the ramping duration for gas compositions and electrical power coincide but other combinations are possible as well, for example power ramping may continue while no further safety gas is used (or vice versa). Simulations were also done with higher rates which may be feasible for the second phase of the start-up procedure, but the present values led to improved numerical stability throughout the entire simulation run. With further optimization of the input values for the controlled variables more aggressive rates are hence applicable. Concerning the balance-of-plant system components, the combustor can be assumed to respond (nearly) instantaneously. Perhaps it needs to be bypassed during start-up to avoid interruptions in the heat supply to the SOFC. For the pre-heater standard materials can be used, i.e., the exhaust gas from the combustor can be directly fed to those process units. The entire start-up procedure from off-mode conditions to operation conditions takes about 12.4 h which is in the range presented in Reference [20].

4.3. Performance and Temperature Response

Figure 8 shows the minimum, mean, and maximum spatial temperature in the SOFC during start-up, with an absolute maximum of 1299 K in the chosen design point. The temperature of the solid eventually exceeds that of the fluids due to the electrochemical reactions, as discussed earlier. Figure 9 shows the maximum of the temperature gradient and temperature difference over the SOFC's axial length in the solid, as well as FU over time. Notice that power ramping and changes in the chemical composition of the feed gases is initiated after the final gas temperatures have been reached (Figures 6 and 7). The decreasing maximum temperature difference shown in Figure 8 can be explained by the dynamic response due to thermal inertia at a constant feed gas temperature during power ramping. With higher concentrations of reactive species in the feed gases, the maximum temperature difference increases again, but without exceeding the specified limit (Table 1). Once power ramping is initiated, the FU changes rapidly (electrical phenomena are modeled such that these occur instantaneously [83]). In (semi-)steady state conditions, the FU reaches 71.5% (Table 2). The pressure of fluid entering the cathode and anode are kept constant, but could in principle be controlled. Here, the pressure difference between cathode and anode channels is kept <0.1 bar (Table 2).

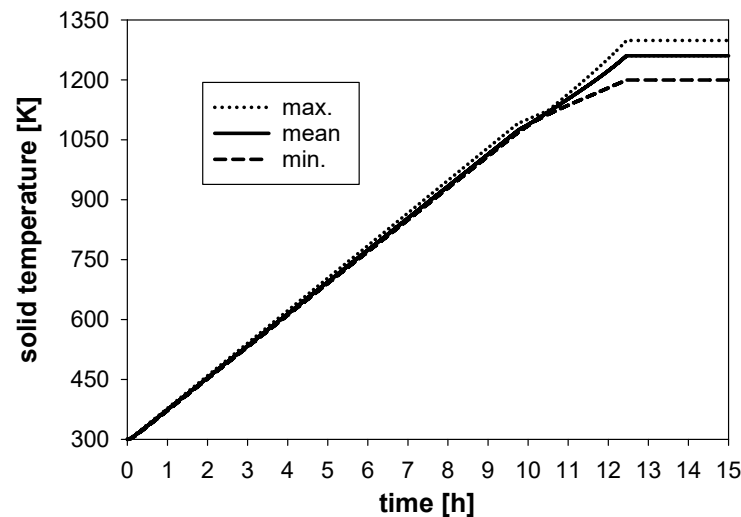


Figure 8. Minimum, mean, and maximum spatial temperature in the solid during start-up.

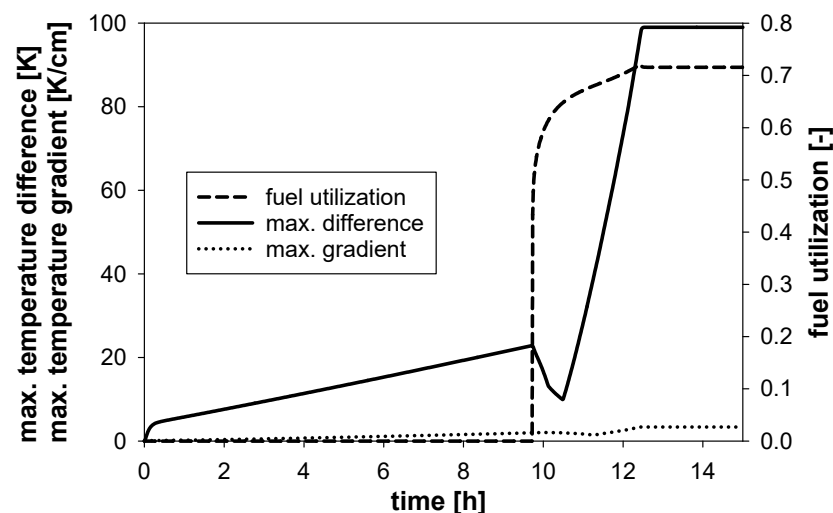


Figure 9. Transient temperature gradient and FU during start-up.

4.4. Stress Distributions and Displacements

Changes in the stresses occur primarily as a result of thermo-elasticity, in other words, any changes that make the force term in the Navier equations larger. Figures 10–12 show the stress distributions for the electrolyte in axial direction in the r -, θ - and z -coordinate, respectively. The profiles represent snapshots at different times of the start-up procedure, starting at ambient and ending at design operation conditions. The stresses decrease with progress in the start-up process because the force term in the equation set describing thermo-mechanics decreases, or more specifically the difference between sintering temperature (manufacturing) and operation temperature, gets smaller. From the two electrode and the electrolyte materials, the largest stresses occur in the latter because of a higher value for the Young's modulus compared to those of the electrodes. As shown in Table 3, the Young's modulus for the electrolyte and anode are modeled as a function of temperature, the absolute maximum in the chosen design point is 159 GPa for the electrolyte and 44.2 GPa for the anode, respectively. On the other hand, the electrolyte's thermal expansion coefficient is lower than those for the electrodes (Table 3), which also directly affects the magnitude of the force terms for thermo-mechanical stresses. However, the Young's modulus dominates over the thermal expansion coefficient.

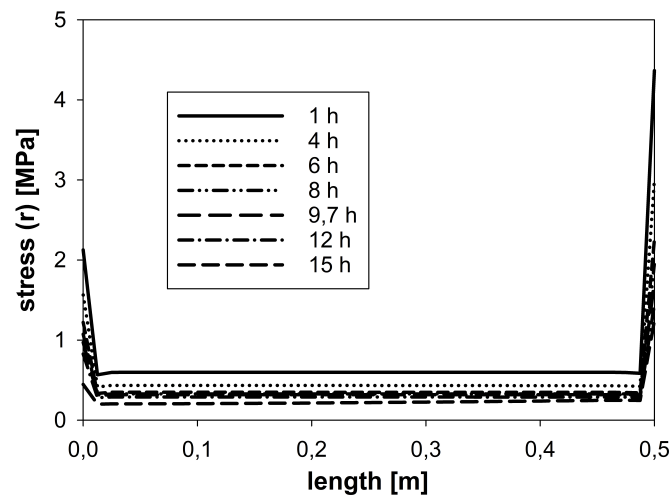


Figure 10. Stresses in electrolyte material for r -coordinate.

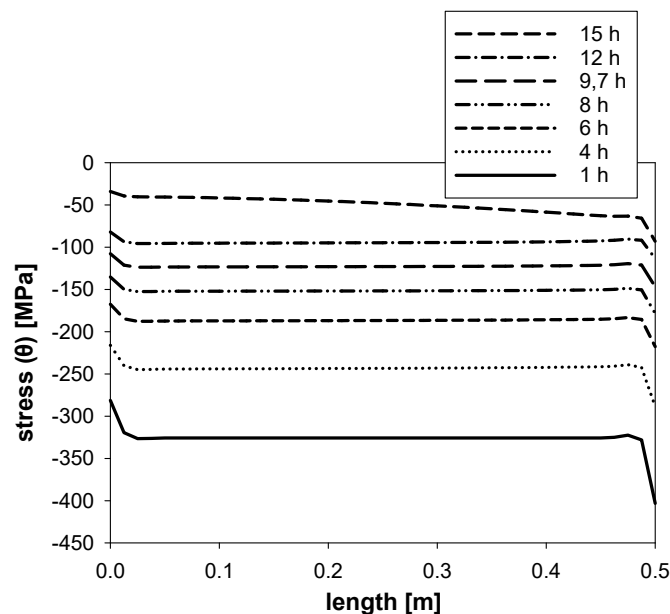


Figure 11. Stresses in electrolyte material for θ -coordinate.

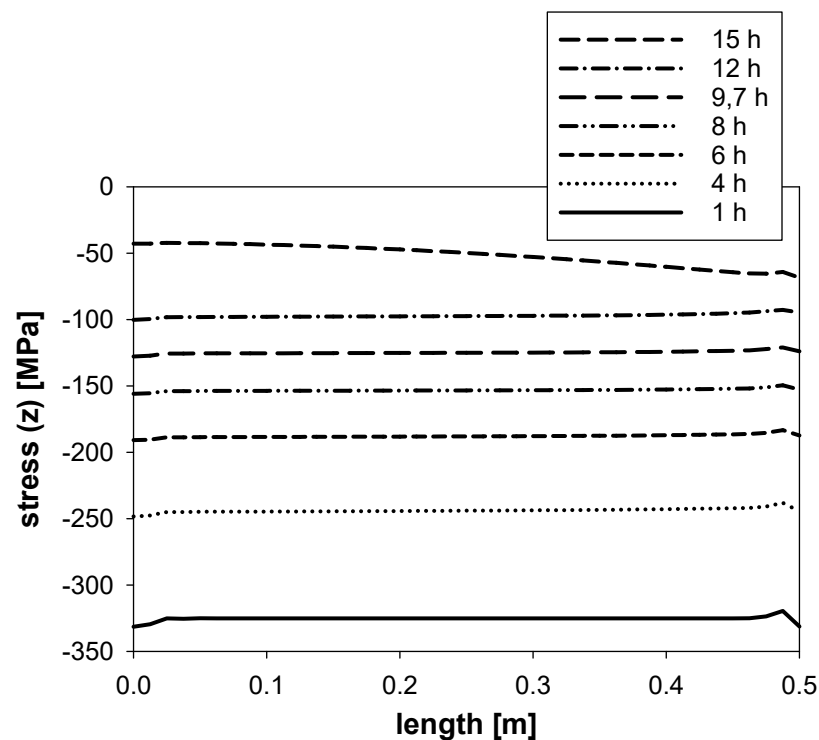


Figure 12. Stresses in electrolyte material for z-coordinate.

Figure 13 shows the displacement distribution in the r - and z -coordinate along the SOFC's axial length for the electrolyte materials under (semi-)steady state conditions in the design point. Absolute values of displacements in the z -coordinate (maximum 1.27 mm) are more than 30 times higher than those for the r -coordinate (maximum 0.037 mm), which can be a problem from a stability point of view. The membrane layer of the SOFC in the present case is cathode-supported (Figure 3), while anode and electrolyte remain unconstrained. The latter parts can, therefore, relax some of the occurring stresses. As discussed previously, the cathode-support is considered in the boundary conditions for the thermo-mechanics, but sealants and their connection on the SOFC housing were not modeled.

Proper matching of physical properties is critical for all physically adjacent materials, including anodes and electrolyte as well as sealants, interconnects and current collectors. Materials in the membrane layer, however, need to meet functional behavior in addition to stability properties. Insufficient stability can lead to failure, for example due to physical disconnection, with potentially severe consequences on a system level. In Table 1 an upper leakage rate limit in the SOFC is specified. Any leakage can lead to a loss of performance, but possibly more critically, it can also pose a potential safety risk if high-temperature combustible gases accumulate outside the designated space over time, which may not be (easily) detectable. In physical systems, a perfect seal is difficult to achieve. The extent of the shift depends on the temperature and other parameters; every temperature gradient leads to a spatial gradient in the materials. Therefore, proper instrumentation for performance monitoring is critical.

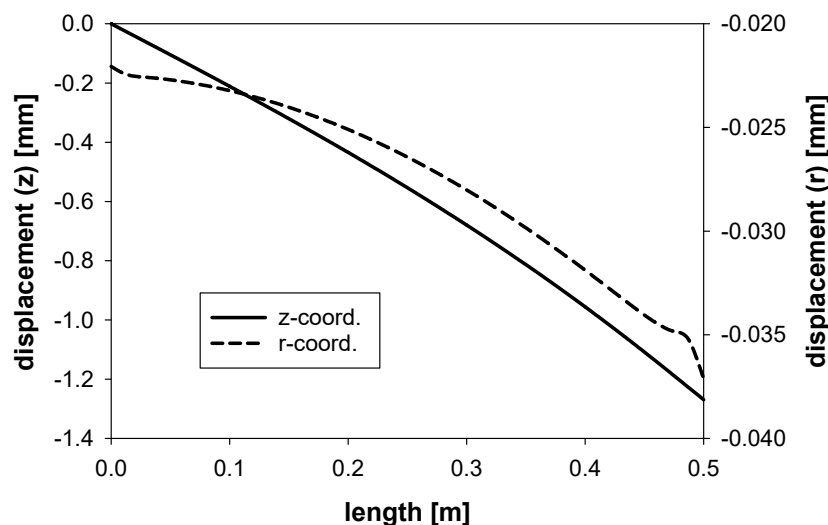


Figure 13. Displacements in electrolyte in design point.

5. Conclusions and Final Remarks

From a practical point of view, the number of conditions that need to be controlled during start-up is relatively extensive, resulting in a complex start-up procedure for the SOFC system. Auxiliary equipment is needed and a further cost factor is the requirement of safety gas considering the total start-up time.

Hydrogen is perhaps the most benign fuel for SOFC in terms of long-term stability. Other fuels such as carbon-containing fuels are more challenging, among others because of the more complex reaction chemistry involved, also with detrimental characteristics such as coke formation. Moreover, using natural gas as feedstock requires additional equipment, such as pre-reformer. Additional requirements need to be considered for concepts comprising other complex sub-processes (for example for internal fuel production) to ensure proper performance and process control, as well as economical perspective.

Thermo-elastic stresses are a problem for SOFC during start-up and shutdown. To moderate stresses during operation at elevated temperatures any changes in values of physical properties or state variables leading to an increased force term of the Navier equations should be minimized. During start-up, the system's temperature goes through a regime of relatively low temperatures for several hours, which lead to high thermo-mechanical stresses. In general, frequent start-up and shutdown cycles should be avoided for economic reasons due to relatively long time periods until reaching design operation conditions, as well as higher risk of failure. Hence, for (thermal) systems comprising delicate process components and parts, transients (start-up and shutdown in particular) need to be considered with a view to thermo-mechanical and chemical stability, in addition to system performance under steady state conditions around the design point.

The application of a multi-physics modeling and simulation approach for the start-up procedure revealed further physical phenomena in the time domain which will be missed with a purely thermodynamic (lumped) approach or state-space models. Fuel cell-based systems are suitable to demonstrate the capabilities of this approach because they comprise thermal, electrochemical, chemical, and mechanical phenomena in a strongly interconnected fashion. Knowledge about the distribution of critical state variables occurring in the system over time can provide useful information for materials scientists as well as systems- and control engineers. Some physical input properties were hard to find, in particular for those having a dependency on state variables, such as temperature.

Potential avenues from this work include the simulation of fuels other than pure hydrogen, which would introduce further constraints. Other geometries than tubular may be modeled and analyzed. Furthermore, the start-up procedure was developed manually

through a trial-and-error approach. The start-up procedure could be formulated as a PDE-constrained optimization problem (perhaps after simplifications of the system model). Control strategies and controller designs may be developed for the entire range of interest, also including start-up and shutdown of the system, for example based on non-linear model predictive control. Physics-based models represent important building blocks for concepts, such as digital twins [84].

Overall, engineering aspects should be taken into account, which make further testing of full-scale systems under realistic conditions indispensable to obtain a better general understanding of the system's dynamics.

Author Contributions: Both authors contributed in all parts. All authors have read and agreed to the published version of the manuscript.

Funding: Please see acknowledgements.

Acknowledgments: Christoph Stiller is gratefully acknowledged for providing the original SOFC performance model code. VVK acknowledges support from the Russian Science Foundation (grant 17-79-30071). KEC acknowledges financial support from NTNU. We thank the editors and anonymous reviewers who made it possible to improve the original manuscript.

Conflicts of Interest: None.

List of symbols

A	area [m ²]
a	activity [-]
C	gas concentration [mol/m ³]
c_p	heat capacity [J/(mol K)]
E	Young's modulus [Pa]
E°	Gibbs potential [V]
F	Faraday constant [C/mol], force [kg/(m s ²)]
FU	fuel utilization [-]
h	enthalpy [J/mol]
h_c	heat transfer coefficient [W/(m ² K)]
i	current density [A/m ²]
I	current [A]
j	index for anode, cathode, electrolyte [-]
L	length [m]
LHV	lower heating value [J/mol]
\dot{m}	mass flow [kg/s]
\dot{n}	mole flow [mol/s]
p	partial pressure [Pa]
P	power [W]
R	universal gas constant [J/(mol K)], ohmic resistance [Ω]
r	radius, spatial distribution variable in radial direction [m]
\dot{r}	reaction rate [mol/s]
t	time [s, h]
u	displacement [m]
v	fluid velocity [m/s]
V	voltage [V]
T	temperature [K]

\tilde{T}	difference between operation and sintering temperature [K]
z	number of electrons [-], spatial distribution variable in axial direction [m]
α	thermal expansion coefficient [1/K]
β	constant for Butler-Volmer equation [-], thermo-mechanical coefficient [Pa/K]
γ	heat capacity ratio [-]
ε	strain [-]
η	overpotential [-], efficiency [-]
λ	thermal conductivity [W/(K m)], Lamé coefficient [Pa]
μ	Lamé coefficient [Pa]
ρ	density [kg/m ³]
ν	Poisson ratio [-]
σ	stress [Pa]
τ	shear stress [Pa]

List of subscripts

<i>act</i>	activation overpotential losses
<i>con</i>	concentration polarisation loss
<i>el</i>	electrical
<i>f</i>	forward reaction
<i>g</i>	gaseous
<i>i</i>	chemical species
<i>OC</i>	open circuit
<i>ohm</i>	ohmic loss
<i>oxi</i>	oxidation
<i>r</i>	reverse reaction, <i>r</i> -coordinate
<i>red</i>	reduction
<i>s</i>	solid
<i>safe</i>	safety gas
<i>TPB</i>	triple-phase boundary
<i>z</i>	spatial <i>z</i> -direction
θ	spatial θ -direction

List of superscripts

<i>an</i>	anode
<i>ca</i>	cathode

List of abbreviations

AC	alternating current
CV	controlled variable(s)
DC	direct current
DOF	degree(s) of freedom
FD	finite difference
FU	fuel utilization
MV	manipulated variable(s)
PDAIE	partial differential algebraic integral equation(s)
SE	systems engineering
SOFC	solid oxide fuel cell(s)
TPB	triple-phase boundary

References

1. Adams, T., II; Nease, J.; Tucker, D.; Barton, P. Energy conversion with solid oxide fuel cell systems: A review of concepts and outlooks for the short- and long-term. *Ind. Eng. Chem. Res.* **2013**, *52*, 3089–3111. [\[CrossRef\]](#)
2. Braun, R.; Klein, S.; Reindl, D. Evaluation of system configurations for solid oxide fuel cell-based micro-combined heat and power generators in residential applications. *J. Power Sources* **2006**, *158*, 1290–1305. [\[CrossRef\]](#)
3. Edwards, P.; Kuznetsov, V.; David, W.; Brandon, N. Hydrogen and fuel cells: Towards a sustainable energy future. *Energy Policy* **2008**, *36*, 4356–4362. [\[CrossRef\]](#)
4. O'Hayre, R.; Cha, S.; Colella, W.; Prinz, F. *Fuel Cell Fundamentals*; John Wiley & Sons: Hoboken, NJ, USA, 2016.
5. Lawlor, V.; Griesser, S.; Buchinger, G.; Olabi, A.; Cordiner, S.; Meissner, D. Review of the micro-tubular solid oxide fuel cell. part I. stack design issues and research activities. *J. Power Sources* **2009**, *193*, 387–399. [\[CrossRef\]](#)
6. Choudhury, A.; Chandra, H.; Arora, A. Application of solid oxide fuel cell technology for power generation—A review. *Renew. Sustain. Energy Rev.* **2013**, *20*, 430–442. [\[CrossRef\]](#)
7. Stambouli, A.; Traversa, E. Solid oxide fuel cells (sofcs): A review of an environmentally clean and efficient source of energy. *Renew. Sustain. Energy Rev.* **2002**, *6*, 433–455. [\[CrossRef\]](#)
8. Zhang, X.; Chan, S.; Li, G.; Ho, H.; Li, J.; Feng, Z. A review of integration strategies for solid oxide fuel cells. *J. Power Sources* **2010**, *195*, 685–702. [\[CrossRef\]](#)
9. Cavalli, A.; Aravind, P. Effect of selected representative biomass gasification tar compounds on ni-gdc solid oxide fuel cells. *Int. J. Hydrog. Energy* **2021**, *46*, 21124–21135. [\[CrossRef\]](#)
10. Jacobson, A. Materials for solid oxide fuel cells. *Chem. Mater.* **2010**, *22*, 660–674. [\[CrossRef\]](#)
11. Kuramoto, K.; Hosokai, S.; Matsuoka, K.; Ishiyama, T.; Kishimoto, H.; Yamaji, K. Degradation behaviors of sofc due to chemical interaction between ni-ysz anode and trace gaseous impurities in coal syngas. *Fuel Process. Technol.* **2017**, *160*, 8–18. [\[CrossRef\]](#)
12. Lanzini, A.; Ferrero, D.; Papurello, D.; Santarelli, M. Reporting degradation from different fuel contaminants in ni-anode sofcs. *Fuel Cells* **2017**, *17*, 423–433. [\[CrossRef\]](#)
13. Martinez, A.; Gerdes, K.; Gemmen, R.; Poston, J. Thermodynamic analysis of interactions between ni-based solid oxide fuel cells (sofc) anodes and trace species in a survey of coal syngas. *J. Power Sources* **2010**, *195*, 5206–5212. [\[CrossRef\]](#)
14. Wang, Y.; Li, W.; Ma, L.; Li, W.; Liu, X. Degradation of solid oxide electrolysis cells: Phenomena, mechanisms, and emerging mitigation strategies—A review. *J. Mater. Sci. Technol.* **2020**, *55*, 35–55. [\[CrossRef\]](#)
15. Peksen, M. Numerical thermomechanical modelling of solid oxide fuel cells. *Prog. Energy Combust. Sci.* **2015**, *48*, 1–20. [\[CrossRef\]](#)
16. Timurkutluk, B.; Mat, M. A performance prediction tool for solid oxide fuel cells after single redox cycle. *Fuel Cells* **2015**, *15*, 71–89. [\[CrossRef\]](#)
17. Xiang, Y.; Da, Y.; Zhong, Z.; Shikazono, N.; Jiao, Z. Thermo-mechanical stress analyses of solid oxide fuel cell anode based on three-dimensional microstructure reconstruction. *Int. J. Hydrog. Energy* **2020**, *45*, 19791–19800. [\[CrossRef\]](#)
18. Chen, M.-H.; Jiang, T. The analyses of the start-up process of a planar, anode-supported solid oxide fuel cell using three different start-up procedures. *J. Power Sources* **2012**, *220*, 331–341. [\[CrossRef\]](#)
19. Zheng, K.; Kuang, Y.; Rao, Z.; Shen, S. Numerical study on the effect of bi-polar plate geometry in the sofc heating-up process. *J. Renew. Sustain. Energy* **2019**, *11*, 014301. [\[CrossRef\]](#)
20. Halinen, M.; Thomann, O.; Kiviaho, J. Experimental study of sofc system heat-up without safety gases. *Int. J. Hydrog. Energy* **2014**, *39*, 552–561. [\[CrossRef\]](#)
21. Choudhary, T.; Sanjay. Computational analysis of ir-sofc: Transient, thermal stress, carbon deposition and flow dependency. *Int. J. Hydrog. Energy* **2016**, *41*, 10212–10227. [\[CrossRef\]](#)
22. Ki, J.; Kim, D. Computational model to predict thermal dynamics of planar solid oxide fuel cell stack during start-up process. *J. Power Sources* **2010**, *195*, 3186–3200. [\[CrossRef\]](#)
23. Al-Masri, A.; Peksen, M.; Blum, L.; Stolten, D. A 3d cfd model for predicting the temperature distribution in a full scale apu sofc short stack under transient operating conditions. *Appl. Energy* **2014**, *135*, 539–547. [\[CrossRef\]](#)
24. Peksen, M.; Al-Masri, A.; Blum, L.; Stolten, D. 3D transient thermomechanical behaviour of a full scale sofc short stack. *Int. J. Hydrog. Energy* **2013**, *38*, 4099–4107. [\[CrossRef\]](#)
25. Peksen, M. Safe heating-up of a full scale sofc system using 3d multiphysics modelling optimisation. *Int. J. Hydrog. Energy* **2018**, *43*, 354–362. [\[CrossRef\]](#)
26. Eapen, D.E.; Suresh, R.; Patil, S.; Rengaswamy, R. A systems engineering perspective on electrochemical energy technologies and a framework for application driven choice of technology. *Renew. Sustain. Energy Rev.* **2021**, *147*, 111165. [\[CrossRef\]](#)
27. Oh, S.-R.; Sun, J.; Dobbs, H.; King, J. Model predictive control for power and thermal management of an integrated solid oxide fuel cell and turbocharger system. *IEEE Trans. Control Syst. Technol.* **2014**, *22*, 911–920.
28. Fergus, J.W. *Solid Oxide Fuel Cells*; John Wiley & Sons, Ltd.: Hoboken, NJ, USA, 2012; chapter 14, pp. 671–700.
29. Gellings, P.J.; Bouwmeester, H.J. *Handbook of Solid State Electrochemistry*; CRC: Boca Raton, FL, USA, 1997.
30. Li, P.-W.; Chyu, M.K. Simulation of the chemical/electrochemical reactions and heat/mass transfer for a tubular sofc in a stack. *J. Power Sources* **2003**, *124*, 487–498. [\[CrossRef\]](#)
31. Colombo, K.W.E.; Kharton, V.V.; Berto, F.; Paltrinieri, N. Mathematical modeling and simulation of hydrogen-fueled solid oxide fuel cell system for micro-grid applications—Effect of failure and degradation on transient performance. *Energy* **2020**, *202*, 117752. [\[CrossRef\]](#)

32. Sammes, N.; Du, Y.; Bove, R. Design and fabrication of a 100w anode supported micro-tubular sofc stack. *J. Power Sources* **2005**, *145*, 428–434. [[CrossRef](#)]
33. Li, G.; Gou, Y.; Qiao, J.; Sun, W.; Wang, Z.; Sun, K. Recent progress of tubular solid oxide fuel cell: From materials to applications. *J. Power Sources* **2020**, *477*, 228693. [[CrossRef](#)]
34. Ho, T.X.; Kosinski, P.; Hoffmann, A.C.; Vik, A. Modeling of transport, chemical and electrochemical phenomena in a cathode-supported sofc. *Chem. Eng. Sci.* **2009**, *64*, 3000–3009. [[CrossRef](#)]
35. Chelmehsara, M.E.; Mahmoudimehr, J. Techno-economic comparison of anode-supported, cathode-supported, and electrolyte-supported sofcs. *Int. J. Hydrog. Energy* **2018**, *43*, 15521–15530. [[CrossRef](#)]
36. Ilbas, M.; Kumuk, B. Numerical modelling of a cathode-supported solid oxide fuel cell (sofc) in comparison with an electrolyte-supported model. *J. Energy Inst.* **2019**, *92*, 682–692. [[CrossRef](#)]
37. Huang, K.; Singhal, S. Cathode-supported tubular solid oxide fuel cell technology: A critical review. *J. Power Sources* **2013**, *237*, 84–97. [[CrossRef](#)]
38. Mueller, F.; Jabbari, F.; Brouwer, J. On the intrinsic transient capability and limitations of solid oxide fuel cell systems. *J. Power Sources* **2009**, *187*, 452–460. [[CrossRef](#)]
39. NETL. *Fuel Cell Handbook*; US Department of Energy, National Energy Technology Laboratory: Morgantown, WV, USA, November 2004
40. Vielstich, W.; Lamm, A.; Gasteiger, H.A. (Eds.) *Handbook of Fuel Cells*; Wiley: Hoboken, NJ, USA, 2009; Volume 5.
41. Vielstich, W.; Lamm, A.; Gasteiger, H.A. (Eds.) *Handbook of Fuel Cells*; Wiley: Hoboken, NJ, USA, 2009; Volume 6.
42. Wu, X.; Gao, D. Optimal robust control strategy of a solid oxide fuel cell system. *J. Power Sources* **2018**, *374*, 225–236. [[CrossRef](#)]
43. Kim-Lohsoontorn, P.; Priyakorn, F.; Wetwatana, U.; Laosiripojana, N. Modelling of a tubular solid oxide fuel cell with different designs of indirect internal reformer. *J. Energy Chem.* **2014**, *23*, 251–263. [[CrossRef](#)]
44. Spivey, B.; Edgar, T. Dynamic modeling, simulation, and mimo predictive control of a tubular solid oxide fuel cell. *J. Process. Control* **2012**, *22*, 1502–1520. [[CrossRef](#)]
45. Jiang, J.; Li, X.; Li, J. Modeling and model-based analysis of a solid oxide fuel cell thermal-electrical management system with an air bypass valve. *Electrochim. Acta* **2015**, *177*, 250–263. [[CrossRef](#)]
46. Chen, J.; Song, W.; Xu, D. Thermal management in catalytic heat-recirculating micro-combustors: A computational fluid dynamics study. *Appl. Therm. Eng.* **2019**, *160*, 114073. [[CrossRef](#)]
47. Karagiannidis, S.; Mantzaras, J.; Jackson, G.; Boulouchos, K.; Hetero-/homogeneous combustion and stability maps in methane-fueled catalytic microreactors. *Proc. Combust. Inst.* **2007**, *31*, 3309–3317. [[CrossRef](#)]
48. Li, Q.; Wang, J.; Meng, L.; Li, J.; Guo, Z. Cfd study on stability limits of hydrogen/air premixed flames in planar micro-combustors with catalytic walls. *Appl. Therm. Eng.* **2017**, *121*, 325–335. [[CrossRef](#)]
49. Shantanu, M.; Reddy, V.M.; Karmakar, S. Experimental and numerical studies on heat recirculated high intensity meso-scale combustor for mini gas turbine applications. *Energy Convers. Manag.* **2018**, *176*, 324–333. [[CrossRef](#)]
50. Wang, Y.; Zhou, Z.; Yang, W.; Zhou, J.; Liu, J.; Wang, Z.; Cen, K. Combustion of hydrogen-air in micro combustors with catalytic pt layer. *Energy Convers. Manag.* **2010**, *51*, 1127–1133. [[CrossRef](#)]
51. Zhou, J.; Wang, Y.; Yang, W.; Liu, J.; Wang, Z.; Cen, K. Combustion of hydrogen-air in catalytic micro-combustors made of different material. *Int. J. Hydrog. Energy* **2009**, *34*, 3535–3545. [[CrossRef](#)]
52. Zhang, X.; Keramati, H.; Arie, M.; Singer, F.; Tiwari, R.; Shooshtari, A.; Ohadi, M. Recent developments in high temperature heat exchangers: A review. *Front. Heat Mass Transf.* **2018**, *11*. [[CrossRef](#)]
53. Fardadi, M.; McLarty, D.; Jabbari, F. Actuator limitations in spatial temperature control of sofc. *J. Fuel Cell Sci. Technol.* **2013**, *10*, 031005. [[CrossRef](#)]
54. Hering, M.; Wahl, S.; Meise, R. Characteristic blower map modeling for volume flow rate estimation in solid oxide fuel cell systems. *Flow Meas. Instrum.* **2018**, *64*, 116–125. [[CrossRef](#)]
55. Cho, J.-H.; Yu, S.-S.; Kim, M.-Y.; Kang, S.-G.; Lee, Y.-D.; Ahn, K.-Y.; Ji, H.-J. Dynamic modeling and simulation of hydrogen supply capacity from a metal hydride tank. *Int. J. Hydrog. Energy* **2013**, *38*, 8813–8828. [[CrossRef](#)]
56. Jiang, J.; Shen, T.; Deng, Z.; Fu, X.; Li, J.; Li, X. High efficiency thermoelectric cooperative control of a stand-alone solid oxide fuel cell system with an air bypass valve. *Energy* **2018**, *152*, 13–26. [[CrossRef](#)]
57. Sorrentino, M.; Pianese, C. Model-based development of low-level control strategies for transient operation of solid oxide fuel cell systems. *J. Power Sources* **2011**, *196*, 9036–9045. [[CrossRef](#)]
58. Sharifzadeh, M. Integration of process design and control: A review. *Chem. Eng. Res. Des.* **2013**, *91*, 2515–2549. [[CrossRef](#)]
59. Stiller, C.; Thorud, B.; Bolland, O.; Kandepu, R.; Imsland, L. Control strategy for a solid oxide fuel cell and gas turbine hybrid system. *J. Power Sources* **2006**, *158*, 303–315. [[CrossRef](#)]
60. Stiller, C. Design, Operation and Control Modelling of SOFC/GT Hybrid Systems. Ph.D. Thesis, Norwegian University of Science and Technology (NTNU), Trondheim, Norway, 2006.
61. Colombo, K.E.; Kharton, V.; Berto, F.; Paltrinieri, N. Mathematical multi-physics modeling and simulation of a solid oxide fuel cell unit for thermo-mechanical stress analyses. *J. Electrochem. Soc.* **2020**, *167*, 044514. [[CrossRef](#)]
62. Colombo, K.E.; Kharton, V.; Berto, F.; Paltrinieri, N. Transient simulation of failures during start-up and power cut of a solid oxide fuel cell system using multiphysics modeling. *Mater. Des. Process. Commun.* **2020**, e177.
63. Bird, R.B.; Stewart, W.E.; Lightfoot, E.N. *Transport Phenomena*; Wiley: Hoboken, NJ, USA, 2006.

64. Hetnarski, R.B.; Eslami, M.R. *Thermal Stresses-Advanced Theory and Applications*; Springer: Berlin/Heidelberg, Germany, 2019.
65. Sadd, M. *Elasticity*, 3rd ed.; Academic Press: Boston, MA, USA, 2009; p. iii.
66. Dwivedi, S. Solid oxide fuel cell: Materials for anode, cathode and electrolyte. *Int. J. Hydrog. Energy* **2020**, *45*, 23988–24013. [[CrossRef](#)]
67. Sreedhar, I.; Agarwal, B.; Goyal, P.; Singh, S.A. Recent advances in material and performance aspects of solid oxide fuel cells. *J. Electroanal. Chem.* **2019**, *848*, 113315. [[CrossRef](#)]
68. Hildenbrand, N.; Boukamp, B.; Nammensma, P.; Blank, D. Improved cathode/electrolyte interface of sofc. *Solid State Ionics* **2011**, *192*, 12–15. [[CrossRef](#)]
69. Greco, F.; Frandsen, H.; Nakajo, A.; Madsen, M.F.; Herle, J.V. Modelling the impact of creep on the probability of failure of a solid oxide fuel cell stack. *J. Eur. Ceram. Soc.* **2014**, *34*, 2695–2704. [[CrossRef](#)]
70. Giraud, S.; Canel, J. Young's modulus of some sofc materials as a function of temperature. *J. Eur. Ceram. Soc.* **2008**, *28*, 77–83. [[CrossRef](#)]
71. Selçuk, A.; Merere, G.; Atkinson, A. The influence of electrodes on the strength of planar zirconia solid oxide fuel cells. *J. Mater. Sci.* **2001**, *36*, 1173–1182. [[CrossRef](#)]
72. Kennouche, D.; Fang, Q.; Blum, L.; Stolten, D. Analysis of the cathode electrical contact in sofc stacks. *J. Electrochem. Soc.* **2018**, *165*, F677–F683. [[CrossRef](#)]
73. Zhang, Y.-C.; Lu, M.-J.; Jiang, W.; Tu, S.-T.; Zhang, X.-C. Effect of the geometrical size on time dependent failure probability of the solid oxide fuel cell. *Int. J. Hydrog. Energy* **2019**, *44*, 11033–11046. [[CrossRef](#)]
74. Boldrin, P.; Ruiz-Trejo, E.; Mermelstein, J.; Menendez, J.B.; Reina, T.R.; Brandon, N. Strategies for carbon and sulfur tolerant solid oxide fuel cell materials, incorporating lessons from heterogeneous catalysis. *Chem. Rev.* **2016**, *116*, 13633–13684. [[CrossRef](#)] [[PubMed](#)]
75. Haga, K.; Adachi, S.; Shiratori, Y.; Itoh, K.; Sasaki, K. Poisoning of sofc anodes by various fuel impurities. *Solid State Ionics* **2008**, *179*, 1427–1431. [[CrossRef](#)]
76. Cheng, Z.; Zha, S.; Liu, M. Influence of cell voltage and current on sulfur poisoning behavior of solid oxide fuel cells. *J. Power Sources* **2007**, *172*, 688–693. [[CrossRef](#)]
77. Hanasaki, M.; Uryu, C.; Daio, T.; Kawabata, T.; Tachikawa, Y.; Lyth, S.; Shiratori, Y.; Taniguchi, S.; Sasaki, K. Sofc durability against standby and shutdown cycling. *J. Electrochem. Soc.* **2014**, *161*, F850–F860. [[CrossRef](#)]
78. Process Systems Enterprise (PSE), the Advanced Process Modelling Company. Available online: <https://www.psenterprise.com/> (accessed on 22 June 2021)
79. *DataFit*; Version 8.2.79; Oakdale Engineering: Oakdale, PA, USA, 2006.
80. Pianko-Oprych, P.; Zinko, T.; Jaworski, Z. Modeling of thermal stresses in a microtubular solid oxide fuel cell stack. *J. Power Sources* **2015**, *300*, 10–23. [[CrossRef](#)]
81. Pianko-Oprych, P.; Zinko, T.; Jaworski, Z. Simulation of thermal stresses for new designs of microtubular solid oxide fuel cell stack. *Int. J. Hydrog. Energy* **2015**, *40*, 14584–14595. [[CrossRef](#)]
82. Colombo, K.W.; Kharton, V.V.; Berto, F.; Paltrinieri, N. Transient system-level performance and thermo-mechanical stress analysis of a solid oxide fuel cell-based power generation plant with a multi-physics approach. *Comput. Chem. Eng.* **2020**, *140*, 106972. [[CrossRef](#)]
83. Schnadt, J.; Bruhwiler, P.; Patthey, L.; O'Shea, J.; Sodergren, S.; Odelius, M.; Ahuja, R.; Karis, O.; Bassler, M.; Persson, P.; et al. Experimental evidence for sub-3-fs charge transfer from an aromatic adsorbate to a semiconductor. *Nature* **2002**, *418*, 620–623. [[CrossRef](#)] [[PubMed](#)]
84. Kang, J.-L.; Wang, C.-C.; Wong, D.S.-H.; Jang, S.-S.; Wang, C.-H. Digital twin model and dynamic operation for a plant-scale solid oxide fuel cell system. *J. Taiwan Inst. Chem. Eng.* **2021**, *118*, 60–67. [[CrossRef](#)]